Eliminating the Interpolation Associated with the Semi-Lagrangian Scheme

HAROLD RITCHIE

Division de Recherche en Prévision Numérique, Service de l'Environnement Atmosphérique, Dorval, Québec, Canada H9P 1J3

(Manuscript received 4 December 1985, in final form 14 August 1985)

ABSTRACT

There are several reasons why it is desirable to eliminate the interpolation associated with the conventional semi-Lagrangian scheme. Interpolation leads to smoothing and is also the most costly operation associated with the technique. Furthermore, its elimination produces a scheme that is more readily adaptable to a spectral model.

In the conventional semi-Lagrangian method, in order to predict a field value at grid point (X_i, Y_j) it is necessary to calculate the trajectory over one time step for the fluid element that arrives at (X_i, Y_j). One then moves along this trajectory in order to extract the field value at an upstream location that generally lies between the grid points, and hence requires the use of interpolation formulae.

This trajectory can be represented as a vector. In the new scheme, the trajectory vector is considered to be the sum of two other vectors—a first vector joining (X_i, Y_j) to the grid point (X_u, Y_u) nearest the upstream location, and a second vector joining (X_u, Y_u) to the upstream location. The advection along the first vector is done via a Lagrangian technique that displaces the field from one grid point to another and, therefore, does not require interpolation. The advection along the second vector is accounted for by an Eulerian approach with the advecting winds modified in such a way that the Courant number is always less than one, thus retaining the attractive stability properties of the interpolating semi-Lagrangian method.

Here the noninterpolating scheme is applied to a model of the shallow water equations and its performance is assessed by comparing the results with those produced by one model which uses the interpolating semi-Lagrangian technique, and another model which uses a fourth-order Eulerian approach. Five-day integrations indicate that the scheme is stable, accurate, and appears to have efficiency advantages.

1. Introduction

The treatment of advection is related to the stability, accuracy, and efficiency of models used in numerical weather prediction. In order to remain stable, Eulerian advection schemes must respect a Courant-Friedrichs-Lewy (CFL) criterion, which limits the size of the time step that can be used in conjunction with a given spatial resolution. However, accuracy considerations suggest another criterion for selecting the size of the time step; that is, the time step should be chosen so that the time truncation errors are comparable to the spatial truncation errors. Eulerian advection schemes would be expected to be inefficient if the maximum time step allowed by the stability constraint is much smaller than that desired on the basis of accuracy. Results obtained using the semi-Lagrangian treatment of advection have demonstrated that this is indeed the case.

Many numerical models have been using integration schemes that have been referred to as "semi-Lagrangian," "upstream advective," or "trajectory methods." For example, see Wiin-Nielsen (1959), Krishnamurti (1962, 1969), Mathur (1970, 1983), Mahrer and Pielke (1978), and Ritchie (1985). In applying such a scheme to the barotropic vorticity equation, Sawyer (1963) found that the results had similar accuracy to those obtained by Eulerian methods and that computational instability of the type associated with the CFL criterion did not arise. Because of its unconditional stability for the advection of Rossby waves, the semi-Lagrangian scheme offers significant computational advantages over the purely Eulerian approach. Robert (1981, 1982) combined this method with the semi-implicit scheme to produce stable and accurate integrations of the shallow water equations with time steps of up to 2 hours. Bates and McDonald (1982) used a semi-Lagrangian approach in a split explicit multilevel primitive equations model. They obtained accurate results using an advection time step of 30 min and an adjustment step of 7.5 min. Robert *et al.* (1985) recently showed that by combining the semi-Lagrangian approach with the semi-implicit scheme, all terms in a multilevel primitive equations model can be treated accurately at high spatial resolution with a time step of 90 minutes. These large time steps are roughly three to six times those permitted by the CFL criterion for the corresponding Eulerian models, showing that the Eulerian stability constraint restricts the time step to one much smaller than that required for accuracy.

Although the semi-Lagrangian scheme permits the use of larger time steps, the overall efficiency of the model is also affected by the use of interpolation, which is the most costly operation associated with the technique. Due to the expense of interpolation, the im-

provement in efficiency is less than the factor by which the time step is increased. This scheme has also been criticized because of the inherent computational damping associated with the interpolation. Furthermore, a noninterpolating version would be more readily adaptable to a spectral model. Thus there are several reasons for eliminating the interpolation associated with the semi-Lagrangian technique; these are the subject of this paper.

The basic difference between the interpolating and noninterpolating versions can be illustrated by considering the one-dimensional advection equation

$$\frac{\partial F}{\partial t} + U\frac{\partial F}{\partial x} = R \tag{1}$$

where U is a constant advecting wind in the x-direction. The Lagrangian formulation results from recognizing that the left-hand side of (1) represents the total derivative of F following a point that is moving with a speed U, yielding

$$\frac{d}{dt}F[x(t), t] = R[x(t), t].$$

In a centered scheme this is approximated as

$$\frac{F[x(t+\Delta t), t+\Delta t] - F[x(t-\Delta t), t-\Delta t]}{2\Delta t} = R[x(t), t].$$

In the usual semi-Lagrangian approach, locations at the forecast time are chosen to be grid points, x_i. Letting α represent the displacement during one time step leads to

$$\frac{F(x_i, t+\Delta t) - F(x_i - 2\alpha, t-\Delta t)}{2\Delta t} = R(x_i - \alpha, t)$$

where $\alpha = \Delta t U$. Generally the upstream locations $x_i - 2\alpha$ and $x_i - \alpha$ will lie between grid points, so that evaluating $F(x_i - 2\alpha, t - \Delta t)$ and $R(x_i - \alpha, t)$ requires the use of interpolation formulae, since only grid point values of the fields are predicted and stored from step to step. In the noninterpolating approach, the advecting wind U in (1) is broken into two parts by adding and subtracting $(p\Delta x)/(2\Delta t)$ where Δx is the grid length, giving

$$\frac{\partial F}{\partial t} + \frac{p\Delta x}{2\Delta t}\frac{\partial F}{\partial x} = -U'\frac{\partial F}{\partial x} + R(x, t) \tag{2}$$

where $U' = U - (p\Delta x)/(2\Delta t)$. The left-hand side now represents the total derivative of F following a point that moves with speed $(p\Delta x)/(2\Delta t)$, so that over two time steps the displacement will be p grid lengths. The residual advection associated with U' appears as an extra term on the right-hand side and, thus, is accounted for in the same way that the total advection would be in an Eulerian treatment. We choose p to give displacement to the grid point nearest $x_i - 2\alpha$ as illustrated in Fig. 1; that is, p is the integer nearest $(2\Delta t U)/(\Delta x)$. After applying the centered semi-Lagrangian approach, (2) becomes

$$\frac{F(x_i, t+\Delta t) - F(x_i - p\Delta x, t-\Delta t)}{2\Delta t} = \left(R - U'\frac{\partial F}{\partial x}\right)\left(x_i - \frac{p\Delta x}{2}, t\right). \tag{3}$$

Since $x_i - p\Delta x$ is a grid point, no interpolation is required to evaluate $F(x_i - p\Delta x, t - \Delta t)$. The right hand side of (3) will be evaluated either at grid points (for p even) or midway between them (for p odd; see Fig. 1).

It should be possible to calculate the residual advection term using either grid point or spectral techniques. In section 2 we use second-order space differencing and extend this formulation to the problem of advection in two dimensions. Since second-order centered space differencing is used in evaluating the residual advection term, and centered differencing is used in assessing the (semi-Lagrangian) time derivative, the resulting scheme can be considered as an upstream generalization of the leap-frog scheme. This approach is shown to be unconditionally stable and nondamping for advection by a constant wind field. Two-dimensional advection tests are presented in section 3 and the accuracy of the new scheme is compared with that of the interpolating semi-Lagrangian version (with cubic interpolations), as well as a fourth-order Eulerian formulation. In section 4 these three treatments of advection are applied to the shallow water equations and the models are compared on 5-day hemispheric integrations. The appendix presents an analysis of the phase characteristics of the noninterpolating semi-Lagrangian scheme applied to the one-dimensional advection equation.

2. Stability analysis

This section presents a stability analysis of the noninterpolating semi-Lagrangian scheme applied to the two-dimensional advection equation

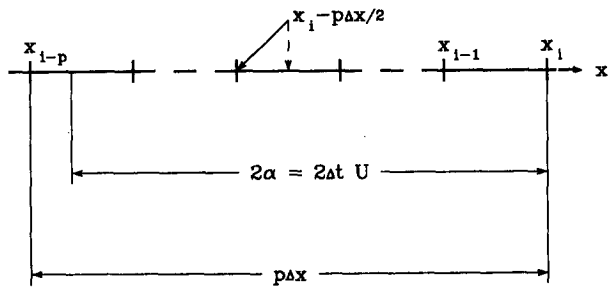

FIG. 1. Schematic diagram illustrating the noninterpolating semi-Lagrangian scheme for the one-dimensional advection problem. $x_i - p\Delta x/2$ is a grid point for p even (solid arrow), or midway between grid points for p odd (dashed arrow).

$$\frac{\partial F}{\partial t} + U\frac{\partial F}{\partial x} + V\frac{\partial F}{\partial y} = 0 \tag{4}$$

where U and V are the x- and y-components of a constant advecting velocity. Following a procedure similar to that for the one-dimensional advection problem, U and V are broken into two parts to give

$$\frac{\partial F}{\partial t} + \frac{p\Delta x}{2\Delta t}\frac{\partial F}{\partial x} + \frac{q\Delta y}{2\Delta t}\frac{\partial F}{\partial y} = -\left(U'\frac{\partial F}{\partial x} + V'\frac{\partial F}{\partial y}\right) \tag{5}$$

where

$$U' = U - \frac{p\Delta x}{2\Delta t}, \quad V' = V - \frac{q\Delta y}{2\Delta t}.$$

The left-hand side of (5) represents the total derivative of F following a point that moves with velocity

$$\left(\frac{p\Delta x}{2\Delta t}, \frac{q\Delta y}{2\Delta t}\right),$$

so that the displacement over two time steps will be p grid lengths in the x-direction and q grid lengths in the y-direction. The residual advection term associated with U' and V' constitutes the right-hand side of (5). In two time steps the actual displacement of field F via (4) will be $(2\Delta tU, 2\Delta tV)$. To give displacement to the nearest grid point, p and q are chosen as the integers nearest $(2\Delta tU)/(\Delta x)$ and $(2\Delta tV)/(\Delta y)$ respectively. The centered Lagrangian approximation of (5) is

$$\{F[x(t+\Delta t), y(t+\Delta t), t+\Delta t] - F[x(t-\Delta t), y(t-\Delta t), t-\Delta t]\}/2\Delta t = -\left(U'\frac{\partial F}{\partial x} + V'\frac{\partial F}{\partial y}\right)[x(t), y(t), t].$$

Choosing locations at the forecast time to be grid points (x_i, y_j) leads to

$$\frac{F(x_i, y_j, t+\Delta t) - F(x_i - p\Delta x, y_j - q\Delta y, t-\Delta t)}{2\Delta t} = -\left(U'\frac{\partial F}{\partial x} + V'\frac{\partial F}{\partial y}\right)\left(x_i - \frac{p\Delta x}{2}, y_j - \frac{q\Delta y}{2}, t\right). \tag{6}$$

Since p and q are integers, no interpolation is required to evaluate $F(x_i - p\Delta x, y_j - q\Delta y, t - \Delta t)$. The locations of the upstream points $(x_i - p\Delta x, y_j - q\Delta y)$ and $(x_i - p\Delta x/2, y_j - q\Delta y/2)$ are given by a straightforward two-dimensional generalization of the locations illustrated by Fig. 1 for the one-dimensional case. We will use second-order space differencing to approximate the derivatives that appear on the right-hand side of (6) and will examine the stability of the scheme by studying *undamped* solutions of the form

$$F = Ce^{i(mx+ny+\omega t)}. \tag{7}$$

The fact that such solutions exist demonstrates that the method is nondamping for advection by a constant wind field.

As a preliminary observation, we note that

$$\frac{U'\Delta t}{\Delta x} = \frac{1}{2}\left(\frac{2\Delta tU}{\Delta x} - p\right)$$

which must be less than ¼ in absolute value, because of the choice we have made for p. A similar statement holds for V', so that

$$\left|\frac{U'\Delta t}{\Delta x}\right| \leq \frac{1}{4}, \quad \left|\frac{V'\Delta t}{\Delta y}\right| \leq \frac{1}{4} \tag{8}$$

where $|\ |$ indicates absolute value. We will also use the notation $F^t_{i,j} \equiv F(i\Delta x, j\Delta y, t)$.

There are four possibilities to consider, depending upon the parities of p and q:

(i) If p and q are both even, the residual advection term is evaluated at grid points and the derivatives can be approximated by the usual centered space forms to give

$$-\left(U'\frac{F^t_{i+1-p/2,j-q/2} - F^t_{i-1-p/2,j-q/2}}{2\Delta x} + V'\frac{F^t_{i-p/2,j+1-q/2} - F^t_{i-p/2,j-1-q/2}}{2\Delta y}\right).$$

Substituting into (6) and looking for a solution in the form of (7) leads to

$$\sin\left(\frac{mp\Delta x}{2} + \frac{nq\Delta y}{2} + \omega\Delta t\right) = -\frac{U'\Delta t}{\Delta x}\sin m\Delta x - \frac{V'\Delta t}{\Delta y}\sin n\Delta y.$$

Reality of ω (i.e., stability) is guaranteed if the "residual Courant number"

$$\left|\frac{U'\Delta t}{\Delta x}\right| + \left|\frac{V'\Delta t}{\Delta y}\right|$$

is less than 1. This is satisfied by virtue of (8), which shows that the value will be less than ½.

(ii) If p is even and q is odd, the point $(x_i - p\Delta x/2, y_j - q\Delta y/2)$ is midway along a line joining adjacent grid points in the y-direction. A second-order approximation to the x-derivative in (6) is given by

$$\frac{1}{2}\left(\frac{F^t_{i+1-p/2,j-(q-1)/2} - F^t_{i-1-p/2,j-(q-1)/2}}{2\Delta x} + \frac{F^t_{i+1-p/2,j-(q+1)/2} - F^t_{i-1-p/2,j-(q+1)/2}}{2\Delta x}\right),$$

while a second-order approximation to the y-derivative in (6) is

$$\frac{F^t_{i-p/2,j-(q-1)/2} - F^t_{i-p/2,j-(q+1)/2}}{\Delta y}.$$

Substituting in (6) and looking for a solution in the form of (7) leads to

$$\sin\left(\frac{mp\Delta x}{2}+\frac{nq\Delta y}{2}+\omega\Delta t\right)$$
$$=-\frac{U'\Delta t}{\Delta x}(\sin m\Delta x)\left(\cos\frac{n\Delta y}{2}\right)-2\frac{V'\Delta t}{\Delta y}\sin\frac{n\Delta y}{2}$$
$$=\left[\left(\frac{U'\Delta t}{\Delta x}\sin m\Delta x\right)^2+\left(\frac{2V'\Delta t}{\Delta y}\right)^2\right]^{1/2}$$
$$\times\sin\left[\frac{n\Delta y}{2}+\tan^{-1}\left(\frac{U'\Delta y}{2V'\Delta x}\sin m\Delta x\right)\right].$$

Stability is guaranteed if the "residual Courant number"

$$\left[\left(\frac{U'\Delta t}{\Delta x}\right)^2+\left(\frac{2V'\Delta t}{\Delta y}\right)^2\right]^{1/2}$$

is less than 1. This is satisfied by virtue of (8), which shows that the value will be less than $5^{1/2}/4 = 0.56$.

(iii) If p is odd and q is even, the point $(x_i - p\Delta x/2, y_j - q\Delta y/2)$ is midway along a line joining two adjacent grid points in the x-direction. Reversing the treatments of the x- and y-derivatives as presented for (ii) yields the "residual Courant number"

$$\left[\left(\frac{2U'\Delta t}{\Delta x}\right)^2+\left(\frac{V'\Delta t}{\Delta y}\right)^2\right]^{1/2}$$

and stability follows as in (ii).

(iv) If p and q are both odd, the point $(x_i - p\Delta x/2, y_j - q\Delta y/2)$ is at the center of a grid rectangle. A second-order approximation to the x-derivative in (6) is given by

$$\frac{1}{2}\left(\frac{F^t_{i-(p-1)/2,j-(q-1)/2}-F^t_{i-(p+1)/2,j-(q-1)/2}}{\Delta x}+\frac{F^t_{i-(p-1)/2,j-(q+1)/2}-F^t_{i-(p+1)/2,j-(q+1)/2}}{\Delta x}\right),$$

while a second order approximation to the y-derivative in (6) is

$$\frac{1}{2}\left(\frac{F^t_{i-(p-1)/2,j-(q-1)/2}-F^t_{i-(p-1)/2,j-(q+1)/2}}{\Delta y}+\frac{F^t_{i-(p+1)/2,j-(q-1)/2}-F^t_{i-(p+1)/2,j-(q+1)/2}}{\Delta y}\right).$$

Substituting in (6) and looking for a solution in the form of (7) leads to

$$\sin\left(\frac{mp\Delta x}{2}+\frac{nq\Delta y}{2}+\omega\Delta t\right)$$
$$=-2\frac{U'\Delta t}{\Delta x}\sin\frac{m\Delta x}{2}\cos\frac{n\Delta y}{2}-2\frac{V'\Delta t}{\Delta y}\cos\frac{m\Delta x}{2}\sin\frac{n\Delta y}{2}$$
$$=-2\left[\left(\frac{U'\Delta t}{\Delta x}\sin\frac{m\Delta x}{2}\right)^2+\left(\frac{V'\Delta t}{\Delta y}\cos\frac{m\Delta x}{2}\right)^2\right]^{1/2}$$
$$\times\sin\left[\frac{n\Delta y}{2}+\tan^{-1}\left(\frac{U'\Delta y}{V'\Delta x}\tan\frac{m\Delta x}{2}\right)\right].$$

By considering the values of m that maximize the radicand in this expression, it can be shown that stability is guaranteed if the "residual Courant number"

$$\max\left\{2\left|\frac{U'\Delta t}{\Delta x}\right|, 2\left|\frac{V'\Delta t}{\Delta y}\right|\right\}$$

is less than 1. This is satisfied by virtue of (8), which shows that the maximum value will be less than ½, thus completing the proof that this scheme is unconditionally stable and nondamping for two-dimensional advection by a constant wind field.

3. Advection tests

To demonstrate the viability of the noninterpolating semi-Lagrangian treatment of advection, two-dimensional advection tests were performed and the accuracy of the new scheme was compared with that of the interpolating semi-Lagrangian version, as well as a fourth-order Eulerian model.

The formulations presented in the previous sections require some slight extensions in order to account for a variable wind field. In a general application (as in the next section) the wind vector (u, v) is a function of space and time, and there is a map scale factor m associated with a conformal projection from the Cartesian (x, y) coordinate system to the (X, Y) coordinate system of the model. In this case the Eulerian formulation of the two-dimensional advection problem is

$$\frac{\partial F}{\partial t}+m^2\left(U\frac{\partial F}{\partial X}+V\frac{\partial F}{\partial Y}\right)=0 \qquad (9)$$

where $(U, V) = (u/m, v/m)$ represents the model wind vector with its components along the (X, Y) coordinates of the model. The Lagrangian version is $dF/dt = 0$ where

$$\frac{d}{dt}=\frac{\partial}{\partial t}+m^2\left(U\frac{\partial}{\partial X}+V\frac{\partial}{\partial Y}\right). \qquad (10)$$

In the centered, interpolating, semi-Lagrangian scheme, if we let the locations at forecast time $t + \Delta t$ be grid points (X_i, Y_j) and let $(\alpha_{ij}, \beta_{ij})$ represent the displacement during one time step, then

$$\frac{dX}{dt}(t)=m^2U(X(t), Y(t), t)$$
$$\frac{dY}{dt}(t)=m^2V(X(t), Y(t), t)$$

lead to

$$\alpha_{ij}=\Delta t(m^2U)(X_i-\alpha_{ij}, Y_j-\beta_{ij}, t)+O(\Delta t^2) \qquad (11)$$

$$\beta_{ij} = \Delta t(m^2 V)(X_i - \alpha_{ij},\ Y_j - \beta_{ij},\ t) + O(\Delta t^2). \quad (12)$$

The two-dimensional advection equation becomes

$$\frac{F(X_i, Y_j, t + \Delta t) - F(X_i - 2\alpha_{ij}, Y_j - 2\beta_{ij}, t - \Delta t)}{2\Delta t} = 0. \quad (13)$$

The noninterpolating semi-Lagrangian version is obtained from the formulation presented in section 2 with (m^2U, m^2V) substituted in the place of (U, V) and (X, Y) instead of (x, y). Thus (6) becomes

$$\frac{F(X_i, Y_j, t + \Delta t) - F(X_i - p\Delta X, Y_j - q\Delta Y, t - \Delta t)}{2\Delta t} = -\left(U' \frac{\partial F}{\partial X} + V' \frac{\partial F}{\partial Y}\right)\left(X_i - \frac{p\Delta X}{2},\ Y_j - \frac{q\Delta Y}{2},\ t\right) \quad (14)$$

where

$$U' = (m^2U)\left(X_i - \frac{p\Delta X}{2},\ Y_j - \frac{q\Delta Y}{2},\ t\right) - \frac{p\Delta X}{2\Delta t} \quad (15)$$

$$V' = (m^2V)\left(X_i - \frac{p\Delta X}{2},\ Y_j - \frac{q\Delta Y}{2},\ t\right) - \frac{q\Delta Y}{2\Delta t}. \quad (16)$$

In order to retain the validity of (8), we choose

$$p = \mathrm{NINT}\left[\frac{2\Delta t}{\Delta X}(m^2U)\left(X_i - \frac{p\Delta X}{2},\ Y_j - \frac{q\Delta Y}{2},\ t\right)\right] \quad (17)$$

$$q = \mathrm{NINT}\left[\frac{2\Delta t}{\Delta Y}(m^2V)\left(X_i - \frac{p\Delta X}{2},\ Y_j - \frac{q\Delta Y}{2},\ t\right)\right] \quad (18)$$

with NINT indicating the nearest integer. Note that (11) and (12) are an implicit set of equations for the displacements α_{ij} and β_{ij}. They require the use of interpolation and are usually solved iteratively. Similarly (17) and (18) give an implicit set of equations for the integer displacements p and q.

Cartesian (x, y) coordinates were used for the tests to be presented in this section, so $m = 1$ here. The advecting wind field was chosen to correspond to solid body rotation of an initial field $f(x, y)$ about a point (x_0, y_0) with constant angular velocity Ω. The analytic solution, found easily by transforming (9) to polar (r, θ) coordinates and using the method of characteristics, can be expressed as

$$F(x, y, t) = f[x_0 + r\cos(\theta - \Omega t),\ y_0 + r\sin(\theta - \Omega t)]$$

where

$$r = [(x - x_0)^2 + (y - y_0)^2]^{1/2}$$

$$\theta = \tan^{-1}[(y - y_0)/(x - x_0)].$$

The initial field was chosen to be a cosine hill function with a peak value of 100 units, drops to zero over a distance of ten grid lengths via

$$50\{1 + \cos[\pi d/(10\Delta x)]\},$$

where d is the distance from the peak, and is zero beyond. We will be using a grid length of 190.5 km, so that this field has a wave length of roughly 3800 km, typical of a synoptic scale feature. The advecting wind field increases linearly as a function of r until it reaches a maximum of approximately 14 m s^{-1}, which is also a typical synoptic scale advection value. This portion of the flow corresponds to solid body rotation and encloses the region in which $F(x, y, t)$ is nonzero. Beyond this radius the wind is tapered smoothly to zero. For these choices, the magnitudes of p and q are 0, 1, 2, or 3. Integrations were carried out for 480 hours, corresponding to approximately one full revolution, and were performed on a grid having 51 points in both the x and y directions.

A comparison was done among the following three models:

(i) The first was an Eulerian model in which a centered time discretization and fourth-order centered space discretization were applied to Eq. (9). For this model, wind speed, and grid length, the CFL stability criterion restricts the time step to less than 2 hours. A time step of 1.5 hours was used here.

(ii) The second was the interpolating semi-Lagrangian version (13) using cubic interpolation. Two iterations were used to solve (11) and (12), and the time step was 6 hours.

(iii) The third was the noninterpolating semi-Lagrangian version (14) in which two iterations were used to solve (17) and (18), and the time step was 6 hours.

A forward step was used to start each integration. The numerical solution at 480 hours produced by the noninterpolating semi-Lagrangian scheme is shown in Fig. 2. This is very close to the corresponding analytic solution, as indicated by the results presented in Table 1. The errors at various times were calculated by comparing to the analytic solution and, as a measure of the accuracy in each case, the integral of the absolute value of these errors was expressed as a percent of the integral of the analytic solution. The error values contained in Table 1 show that all three models were very accurate in solving the two-dimensional advection problem for these wind and space scales that are typical of synoptic features. The time step for the semi-Lagrangian models was four times that of the Eulerian one, and yet they performed with comparable accuracy, thus showing that the CFL stability constraint restricts the time step to one much smaller than is required for accuracy. In particular, the noninterpolating semi-Lagrangian scheme produces stable, accurate integrations, and hence appears to be a viable treatment of advection.

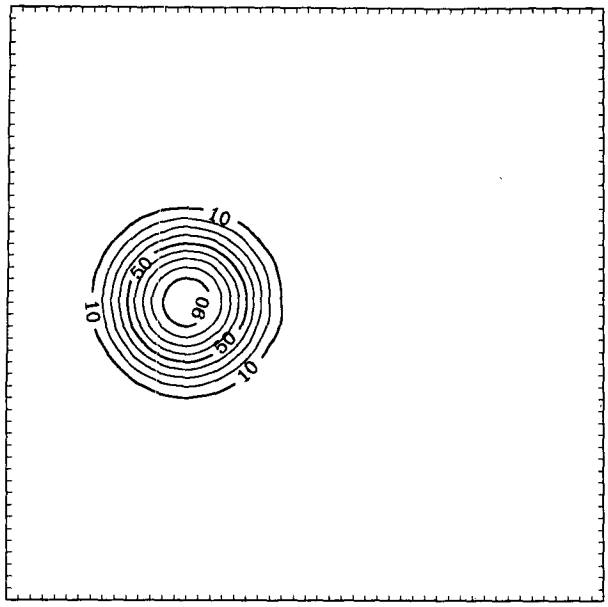

FIG. 2. Numerical solution at 480 hours produced by the noninterpolating semi-Lagrangian scheme for the two-dimensional advection test. Contour interval 10 units.

4. Application to the shallow water equations

In this section the Eulerian, interpolating semi-Lagrangian, and noninterpolating semi-Lagrangian treatments of advection are applied to the shallow water equations

$$\frac{dU}{dt} - fV + \frac{\overline{\partial\phi}^t}{\partial X} + K\frac{\partial S}{\partial X} = 0 \tag{19}$$

$$\frac{dV}{dt} + fU + \frac{\overline{\partial\phi}^t}{\partial Y} + K\frac{\partial S}{\partial Y} = 0 \tag{20}$$

$$\frac{d\phi}{dt} + \phi_0\bar{D}^t + (\phi - \phi_0)D = 0. \tag{21}$$

These equations describe the motion of a hydrostatic, homogeneous, incompressible fluid on a rotating sphere; X, Y, d/dt, U, and V are the same as defined in section 3, ϕ is the geopotential of the free upper surface of the fluid, f is the Coriolis parameter, $S = m^2$ is the square of the map scale factor,

$$\left.\begin{aligned} K &= \tfrac{1}{2}(U^2 + V^2), \\ D &= S(\partial U/\partial X + \partial V/\partial Y) \end{aligned}\right\}.$$

Also, ϕ_0 is a constant roughly equal to the mean value of ϕ and $\overline{(\ )}^t$ denotes a time averaging associated with the semi-implicit treatment of the terms that produce gravity waves.

The performances of three models of the shallow water equations will be compared. The Eulerian model uses a centered time discretization and fourth-order centered space discretization to treat the $d(\ )/dt$ terms in (19) to (21), and $\overline{(\ )}^t$ is defined via

$$\bar{F}^t = \tfrac{1}{2}[F(X_i, Y_j, t + \Delta t) + F(X_i, Y_j, t - \Delta t)]$$

where (X_i, Y_j) represents a grid point. The interpolating semi-Lagrangian model treats the $d(\ )/dt$ terms in the manner presented by (11)–(13), and $\overline{(\ )}^t$ is defined as a time average along the trajectory; that is,

$$\bar{F}^t = \tfrac{1}{2}[F(X_i, Y_j, t + \Delta t) + F(X_i - 2\alpha_{ij}, Y_j - 2\beta_{ij}, t - \Delta t)].$$

In the noninterpolating semi-Lagrangian model, $d(\ )/dt$ terms are handled as in (14)–(16), and $\overline{(\ )}^t$ is given by

$$\bar{F}^t = \tfrac{1}{2}[F(X_i, Y_j, t + \Delta t) + F(X_i - p\Delta X, Y_j - q\Delta Y, t - \Delta t)].$$

Since the general structure is similar for all three models, further details will be given for only the third version. In this case, (19) leads to

$$\left(U + \Delta t\frac{\partial\phi}{\partial X}\right)(X_i, Y_j, t + \Delta t) = \left(U - \Delta t\frac{\partial\phi}{\partial X}\right)(X_i - p\Delta X, Y_j - q\Delta Y, t - \Delta t) + 2\Delta t\left[fV - K\frac{\partial S}{\partial X} - \left(U'\frac{\partial U}{\partial X} + V'\frac{\partial U}{\partial Y}\right)\right], \quad X_i - \frac{p\Delta X}{2}, Y_j - \frac{q\Delta Y}{2}, t; \tag{22}$$

(20) becomes

$$\left(V + \Delta t\frac{\partial\phi}{\partial Y}\right)(X_i, Y_j, t + \Delta t) = \left(V - \Delta t\frac{\partial\phi}{\partial Y}\right)(X_i - p\Delta X, Y_j - q\Delta Y, t - \Delta t)$$

TABLE 1. Error results for the two-dimensional advection test as explained in the text. NISL denotes the noninterpolating semi-Lagrangian model (time step 6 h), ISL the interpolating semi-Lagrangian model (time step 6 h), and EUL the Eulerian model (time step 1.5 h). Errors are expressed in percent.

Time (h)	Model		
	NISL	ISL	EUL
120	1.3	1.1	1.9
240	2.4	2.1	2.8
360	3.4	3.0	3.6
480	4.5	3.9	4.2

$$+ 2\Delta t\left[-fU - K\frac{\partial S}{\partial Y} - \left(U'\frac{\partial V}{\partial X} + V'\frac{\partial V}{\partial Y}\right)\right]$$
$$X_i - \frac{p\Delta X}{2}, Y_j - \frac{q\Delta Y}{2}, t; \quad (23)$$

and (21) gives

$$(\phi + \Delta t\phi_0 D)(X_i, Y_j, t + \Delta t)$$
$$= (\phi - \Delta t\phi_0 D)(X_i - p\Delta X, Y_j - q\Delta Y, t - \Delta t)$$
$$+ 2\Delta t\left[-(\phi - \phi_0)D - \left(U'\frac{\partial \phi}{\partial X} + V'\frac{\partial \phi}{\partial Y}\right)\right]$$
$$X_i - \frac{p\Delta X}{2}, Y_j - \frac{q\Delta Y}{2}, t. \quad (24)$$

As discussed in section 2, depending upon the parities of p and q the point $(X_i - p\Delta X/2, Y_j - q\Delta Y/2)$ may be a grid point, lie midway along a line joining adjacent grid points in either the X- or Y-directions, or lie at the center of a grid rectangle. When the location is between grid points, a second-order approximation to the required value is found by taking an appropriate average of the values at neighboring grid points. The marching procedure for a model time step will now be outlined. Given U, V and ϕ on grid points at times $t - \Delta t$ and t, (17) and (18) can be solved for the integer displacements p and q, following which the right-hand sides of (22) to (24) can be evaluated. Let Q_1, Q_2, and Q_3 denote these right-hand sides respectively, so that the system becomes

$$\left(U + \Delta t\frac{\partial \phi}{\partial X}\right)(X_i, Y_j, t + \Delta t) = Q_1 \quad (25)$$

$$\left(V + \Delta t\frac{\partial \phi}{\partial Y}\right)(X_i, Y_j, t + \Delta t) = Q_2 \quad (26)$$

$$(\phi + \Delta t\phi_0 D)(X_i, Y_j, t + \Delta t) = Q_3. \quad (27)$$

Eliminating D leads to the following Helmholtz equation, which is solved for $\phi(X_i, Y_j, t + \Delta t)$ via an alternating directions implicit scheme

$$\frac{\partial^2 \phi}{\partial X^2} + \frac{\partial^2 \phi}{\partial Y^2} - \frac{1}{\Delta t^2 \phi_0 S}\phi$$
$$= \frac{1}{\Delta t}\left(\frac{\partial Q_1}{\partial X} + \frac{\partial Q_2}{\partial Y}\right) - \frac{Q_3}{\Delta t^2 \phi_0 S}.$$

The time step is then completed by determining $U(X_i, Y_j, t + \Delta t)$ and $V(X_i, Y_j, t + \Delta t)$ via (25) and (26).

The three models were run to produce five-day forecasts on a 117 by 117 point hemispheric grid having a grid length of 190.5 km at 60°N on a polar stereographic projection. In order to reduce the cross-flow on the model boundaries, the initial data was modified to have zero winds and constant geopotential south of 10°N. Between 10° and 20°N the data was blended to vary smoothly from the constant values at 10°N to the unmodified values at 20°N, following a procedure similar to that used by Verner and Benoit (1984). After this massaging, the amplitudes of the gravity waves were reduced by performing a reverse balance equation initialization. The centered time scheme requires field values at times $t = 0$ and $t = \Delta t$ in order to start. The values at $t = \Delta t$ were provided by a slow start procedure, which uses a forward step to produce values at $t = \Delta t/2$, followed by a centered step to give the required values at $t = \Delta t$. The models also included a weak time filter of the type analyzed by Asselin (1972), with a coefficient of 0.04. For the Eulerian model the time step was 20 min, which respects the CFL limit, while the semi-Lagrangian models used a time step of one hour.

"Identical triplet" experiments were performed in an attempt to show that there is little difference among corresponding fields forecast by the three models. This was done for two cases.

The first case started with an analysis valid at 1200 GMT 28 February 1984 for which the initialized 500 mb geopotential field is shown in Fig. 3. Forecasts of the 500 mb geopotential after 24 h are shown in Figs. 4, 5, and 6 as produced by the Eulerian, noninterpolating semi-Lagrangian, and interpolating semi-Lagrangian models, respectively. The corresponding forecasts after 120 h are shown in Figs. 7, 8 and 9. A comparison of these figures shows good agreement on the positions and intensities of all the height centers. The maximum differences among the indicated central values are 2 dam at 24 h and 3 dam at 120 h. In particular, note the similar performances for the 530 dam low that is centered south of the Great Lakes in Fig. 3 and intensifies rapidly as it moves northeastward during

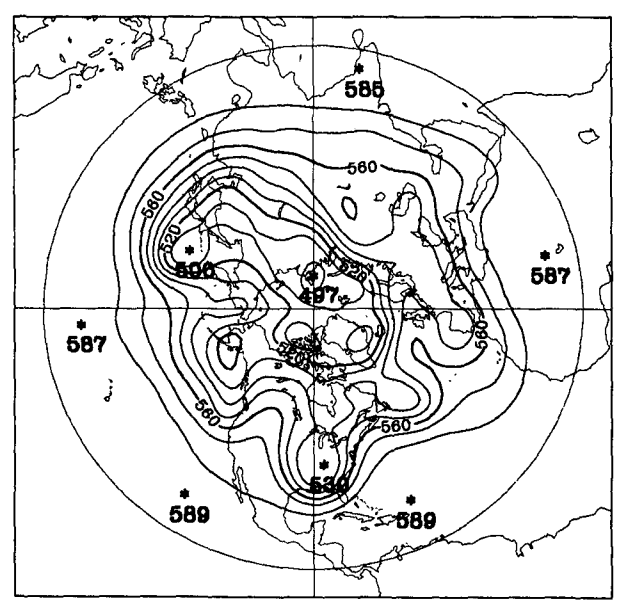

FIG. 3. 500 mb geopotential. 1200 GMT 28 February 1984. Contour interval 10 dam.

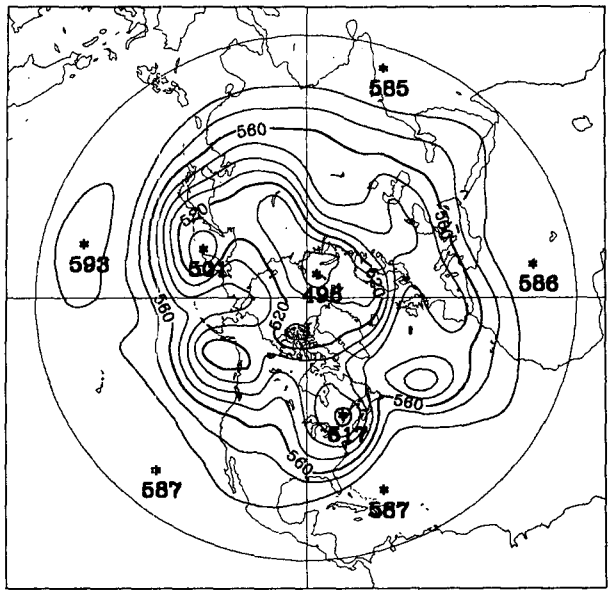

FIG. 4. Eulerian model 24 h forecast of the 500 mb geopotential. 1200 GMT 29 February 1984. Contour interval 10 dam.

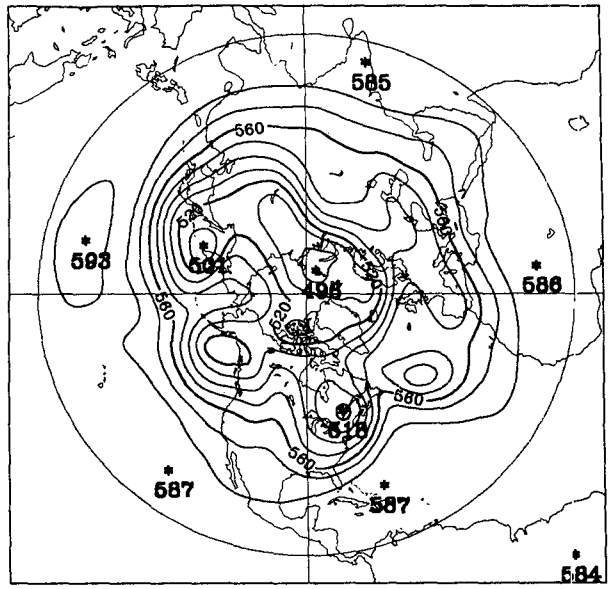

FIG. 6. Interpolating semi-Lagrangian model 24 h forecast of the 500 mb geopotential. 1200 GMT 29 February 1984. Contour interval 10 dam.

the first 24 h. Standard deviations of the differences among these forecasts were calculated and are presented in Table 2. These results are expressed in meters and are area-weighted values for the region north of 20°N, thus excluding the domain in which the initial data was massaged. They show that the accuracy of the noninterpolating semi-Lagrangian treatment of advection is quite acceptable in comparison with the other two treatments. At 24 h the difference is 4.68 m with respect to the Eulerian model, and 3.53 m with respect to the interpolating semi-Lagrangian one; at 120 h these values have increased to 27.90 m and 21.73 m, respectively. In this instance the best agreement is between the interpolating semi-Lagrangian model and the Eulerian one, with differences of 3 m at 24 h and 15.81 m at 120 h. This, however, is not always the case, as shown by the following results.

A second experiment was performed starting with

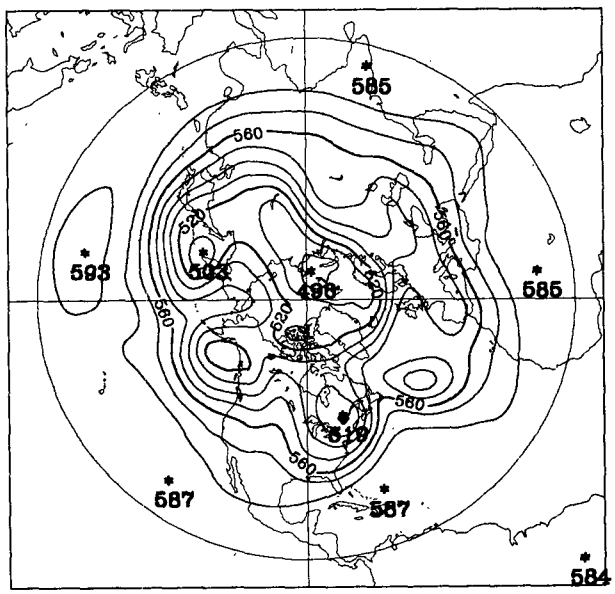

FIG. 5. Noninterpolating semi-Lagrangian model 24 h forecast of the 500 mb geopotential. 1200 GMT 29 February 1984. Contour interval 10 dam.

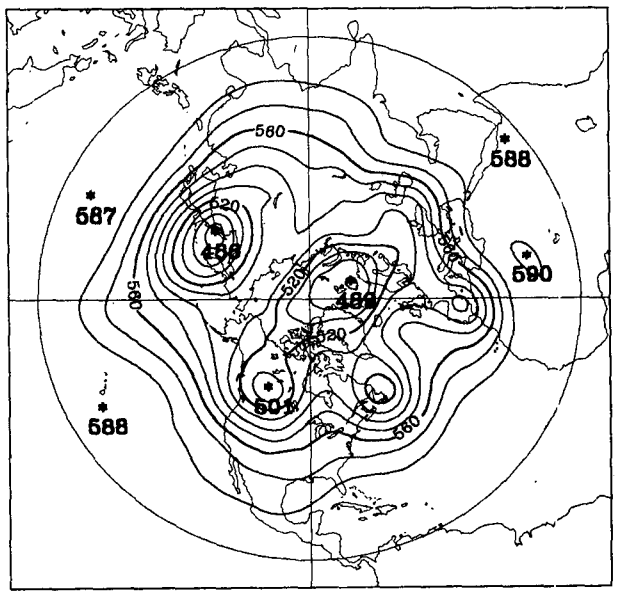

FIG. 7. Eulerian model 120 h forecast of the 500 mb geopotential. 1200 GMT 4 March 1984. Contour interval 10 dam.

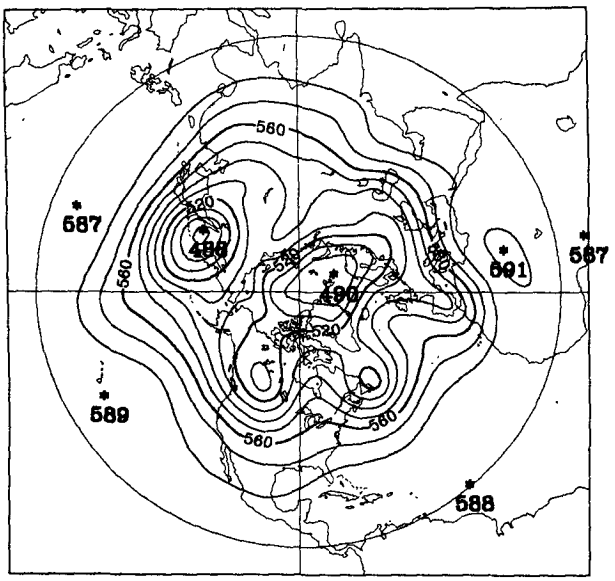

FIG. 8. Noninterpolating semi-Lagrangian model 120 h forecast of the 500 mb geopotential. 1200 GMT 4 March 1984. Contour interval 10 dam.

an analysis valid at 1200 GMT 14 March 1984. Figure 10 gives the 120 h forecast of the 500 mb geopotential from the noninterpolating semi-Lagrangian model, and the differences among the forecasts produced by the three models are presented in Table 3. In this case the differences are less than those presented in Table 2 and the two semi-Lagrangian models show the best agreement at the end of the forecast.

TABLE 2. Standard deviations of the differences among forecasts of the 500 mb geopotential as produced by the three models of the shallow water equations for the case starting from 1200 GMT 28 February 1984. NISL denotes the noninterpolating semi-Lagrangian model (time step 1 h), ISL the interpolating semi-Lagrangian model (time step 1 h), and EUL the Eulerian model (time step 20 min). The results are expressed in meters and are area weighted values for the region north of 20°N.

	Time (h)					
	0	24	48	72	96	120
NISL cf EUL	0.29	4.68	7.54	12.22	21.71	27.90
NISL cf ISL	0.34	3.53	7.31	11.42	19.11	21.73
ISL cf EUL	0.19	3.00	5.21	8.53	12.00	15.81

In these two cases the magnitudes of p and q for the noninterpolating semi-Lagrangian model were typically 0, 1, or 2.

These results demonstrate that the noninterpolating semi-Lagrangian scheme can be accurately and stably applied to the shallow water equations using a time step much larger than that allowed by the CFL limit for the Eulerian model.

5. Discussion

The foregoing sections have examined the elimination of the interpolation associated with the semi-Lagrangian technique. Section 1 outlined the means whereby the advecting wind can be split into two parts such that one part gives displacement to a grid point during two time steps, and the residual advection as-

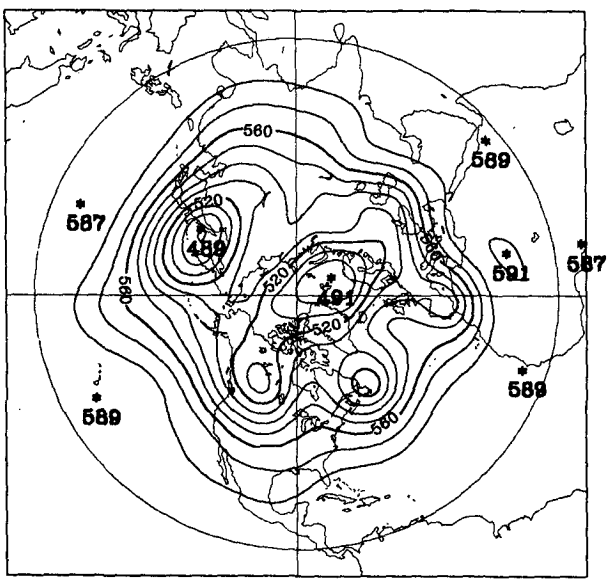

FIG. 9. Interpolating semi-Lagrangian model 120 h forecast of the 500 mb geopotential. 1200 GMT 4 March 1984. Contour interval 10 dam.

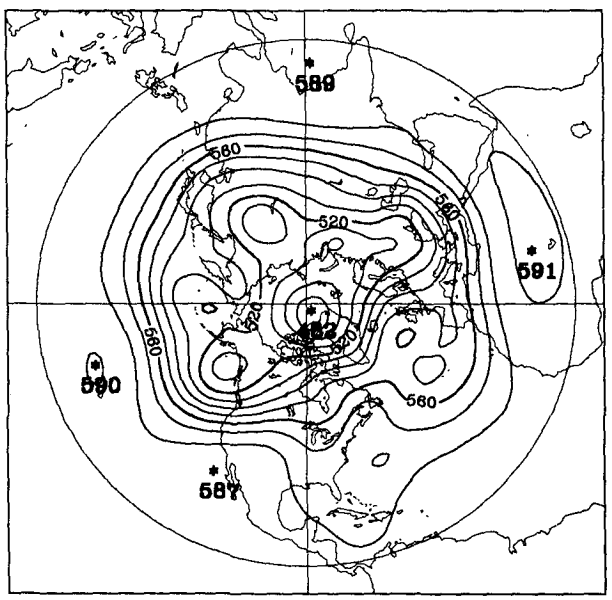

FIG. 10. Noninterpolating semi-Lagrangian model 120 h forecast of the 500 mb geopotential. 1200 GMT 19 March 1984. Contour interval 10 dam.

TABLE 3. As in Table 2 except that the results are for the case starting from 1200 GMT 14 March 1984.

	Time (h)					
	0	24	48	72	96	120
NISL cf EUL	0.21	3.27	5.87	9.04	13.29	19.06
NISL cf ISL	0.25	2.50	4.62	6.98	9.54	13.32
ISL cf EUL	0.13	2.44	3.79	6.52	10.81	14.95

sociated with the second part is accounted for by an Eulerian approach. In section 2 the residual advection term was treated using second-order space differencing and the resulting scheme was shown to be unconditionally stable and nondamping for the problem of two dimensional advection by a constant wind. The two-dimensional advection tests that were presented in section 3 indicate that this is a viable treatment of advection. The noninterpolating formulation was compared with an interpolating semi-Lagrangian version that uses cubic interpolation, as well as with a fourth-order Eulerian version. The time step for the semi-Lagrangian models was much larger than the maximum allowed by the CFL constraint for the Eulerian model, and yet all three models performed with comparable accuracy for typical synoptic values of wind speed and wavelength. There are no apparent problems with the splitting of the advecting wind into two parts that are treated differently, as outlined above. In section 4 these three treatments of advection were applied to the shallow water equations and the models were compared on 5-day hemispheric integrations. "Identical triplet" experiments were presented and indicated that there is little difference among corresponding fields forecast by the three models. Thus it was demonstrated that the noninterpolating semi-Lagrangian scheme can be stably applied to the shallow water equations using a time step much larger than that allowed by the CFL limit for the Eulerian model. It also gives an accuracy that is quite acceptable in comparison with the other two models.

Here the residual advection terms were treated with only second-order space differencing, whereas with cubic interpolation the interpolating semi-Lagrangian scheme was fourth order in space, as was the fully Eulerian treatment of advection. Undoubtedly, for some length scales and time steps, the second-order scheme will pay an accuracy penalty in comparison to the fourth-order schemes. As indicated by the analysis presented in the appendix, the dominant error in this noninterpolating semi-Lagrangian scheme is the phase error associated with the second-order space differencing applied to the residual advection term, even though this error is less than that of a conventional second order leap-frog treatment of advection. The maximum residual Courant number calculated in section 2 was 0.56, while stability is guaranteed for values of less than 1. This leaves room for extending the scheme to advection in three dimensions and/or increasing the order of accuracy of the residual advection calculation. However, the results presented in section 4 indicate that the accuracy of the current scheme is adequate for atmospheric models with typical spatial resolution.

Because the rotation terms fV in (19) and fU in (20) have been treated explicitly, the shallow water equations models also have to respect a stability limit associated with the Coriolis parameter. It was for this reason that time steps larger than one hour were not used with the semi-Lagrangian models. This restriction could be removed by a semi-implicit treatment of the rotation terms as in Robert, 1982. However, as numerical weather prediction models move toward higher spatial resolution, it is quite likely that time steps shorter than one hour will be desired on the basis of accuracy alone. As the spatial resolution gets finer, there will be a corresponding reduction in the maximum time step allowed by the CFL criterion, and the semi-Lagrangian schemes will retain their computational advantage.

The execution times for the integrations that have been presented here indicate that a significant increase in efficiency results from eliminating the interpolation associated with the semi-Lagrangian scheme. However, these models are not fully vectorized yet and it would be misleading to present specific timings before a careful vectorization has been done. Preliminary tests carried out so far indicate that, with the possible exception of gathering operations, both the interpolating and noninterpolating semi-Lagrangian schemes can be fully vectorized.

Acknowledgments. The author wishes to express his deep gratitude to Dr. André Robert for suggesting this project and for many helpful discussions during the course of this work. The experiments in section 4 were performed with modified versions of models that were developed during the study presented by Robert, Yee and Ritchie (1985).

APPENDIX

Phase Characteristics Analysis

This appendix presents an analysis of the phase characteristics of the noninterpolating semi-Lagrangian (NISL) scheme applied to the one-dimensional advection equation

$$\frac{\partial F}{\partial t} + U\frac{\partial F}{\partial x} = 0 \qquad \text{(A1)}$$

where U is a constant advecting wind in the x-direction. Applying the NISL scheme as outlined in the Introduction leads to

$$\frac{F(x_i, t + \Delta t) - F(x_i - p\Delta x, t - \Delta t)}{2\Delta t} = -U'\frac{\partial F}{\partial x}\left(x_i - \frac{p\Delta x}{2}, t\right) \qquad \text{(A2)}$$

where

$$U' = U - \frac{p\Delta x}{2\Delta t} \tag{A3}$$

$$p = \text{NINT}(2U\Delta t/\Delta x) \tag{A4}$$

with NINT indicating the nearest integer. We will use second-order space differencing to approximate $\partial F/\partial x$ as

$$\frac{F\left(x_i - \frac{p\Delta x}{2} + \Delta x, t\right) - F\left(x_i - \frac{p\Delta x}{2} - \Delta x, t\right)}{2\Delta x}$$

for p even, and

$$\frac{F\left(x_i - \frac{p\Delta x}{2} + \frac{\Delta x}{2}, t\right) - F\left(x_i - \frac{p\Delta x}{2} - \frac{\Delta x}{2}, t\right)}{\Delta x}$$

for p odd. Looking for *undamped* solutions of the form

$$F = Ae^{ik(x-Ct)}, \tag{A5}$$

substituting into (A2) and solving for the numerical phase speed C leads to

$$C = \frac{p\Delta x}{2\Delta t} + \frac{1}{k\Delta t}\sin^{-1}\left(\frac{U'\Delta t}{\Delta x}\sin k\Delta x\right) \tag{A6}$$

for p even, and

$$C = \frac{p\Delta x}{2\Delta t} + \frac{1}{k\Delta t}\sin^{-1}\left(\frac{U'\Delta t}{\Delta x}2\sin\frac{k\Delta x}{2}\right) \tag{A7}$$

for p odd. The fact that solutions of the form (A5) exist demonstrates that the method is nondamping for advection by a constant wind. As a consequence of (A3) and (A4) the residual Courant number satisfies

$$\left|\frac{U'\Delta t}{\Delta x}\right| \leq \frac{1}{4}, \tag{A8}$$

so C is real and the scheme is unconditionally stable. The numerical phase speed for the conventional second-order centered time and centered space (CTCS) scheme results from taking $p = 0$ in (A6). Thus the phase speed expression for the NISL scheme is the sum of two terms, the first one ($p\Delta x/2\Delta t$) corresponding to semi-Lagrangian advection to the grid point nearest the upstream point, and the second one corresponding to the phase speed associated with the residual advection. An analytic solution to (A1) is given by (A5) provided that the phase speed is given by $C = U$. From (A3) and (A8) it follows that

$$U\left(1 - \frac{1}{4}\frac{\Delta x}{U\Delta t}\right) \leq \frac{p\Delta x}{2\Delta t} \leq U\left(1 + \frac{1}{4}\frac{\Delta x}{U\Delta t}\right), \tag{A9}$$

showing that, by virtue of the choice made for p, the first term accounts for all but a fraction 1/(4CN) of the analytic phase speed U, where CN is the (total) Courant number $U\Delta t/\Delta x$.

For $k\Delta x$ small, retaining up to second-order terms in the expansion for C leads to

$$C \approx U - U'\left[1 - \left(\frac{U'\Delta t}{\Delta x}\right)^2\right]\frac{(k\Delta x)^2}{6} \tag{A10}$$

for p even, and

$$C \approx U - U'\left[\frac{1}{4} - \left(\frac{U'\Delta t}{\Delta x}\right)^2\right]\frac{(k\Delta x)^2}{6} \tag{A11}$$

for p odd. Recalling (A8), we note that the numerical phase speed C will be less than the analytic phase speed U if U' is positive, and will be greater than U if U' is negative. This is to be contrasted with the conventional CTCS result obtained by setting $p = 0$, for which $U' = U$ and the numerical phase speed will always be less than the analytic one in absolute value. It is also seen from (A8), (A10) and (A11) that the dominant error in this NISL scheme is the phase error ($U'k^2\Delta x^2/6$ for p even; $U'k^2\Delta x^2/24$ for p odd) associated with the second-order space differencing applied to the residual advection term.

There will be a dispersion error resulting from the fact that waves of different wavelength $L = 2\pi/k$ travel with different numerical phase speeds, whereas the phase speed of the analytic solution is U for all wavelengths. For Eulerian advection this is especially noticeable for the short waves. The shortest wave resolvable on a grid has a wavelength $2\Delta x$, and the behavior of the phase speed in this short wave limit is also of interest. This limit corresponds to $\theta \equiv k\Delta x = \pi$, and when expressed in terms of θ, (A6) and (A7) become

$$C = \frac{p\Delta x}{2\Delta t} + \frac{1}{\theta}\left(\frac{\Delta x}{\Delta t}\right)\sin^{-1}\left(\frac{U'\Delta t}{\Delta x}\sin\theta\right) \tag{A12}$$

for p even, and

$$C = \frac{p\Delta x}{2\Delta t} + \frac{1}{\theta}\left(\frac{\Delta x}{\Delta t}\right)\sin^{-1}\left(\frac{U'\Delta t}{\Delta x}2\sin\frac{\theta}{2}\right) \tag{A13}$$

for p odd. Expanding (A12) for θ near π shows that, for p even, the numerical phase speed approaches $p\Delta x/(2\Delta t)$. For the conventional CTCS scheme, $p = 0$, so the two grid-length wave is stationary. If p is nonzero and even, then by (A9), the phase speed will be within a fraction 1/(4CN) of the analytic value U. Expanding (A13) for θ near π shows that, for p odd, the numerical phase speed approaches

$$C_{\text{odd}}(\pi) = \frac{p\Delta x}{2\Delta t} + \frac{1}{\pi}\left(\frac{\Delta x}{\Delta t}\right)\sin^{-1}\left(2\frac{U'\Delta t}{\Delta x}\right). \tag{A14}$$

Using (A8) and (A9) it can be shown that

$$U\left(1 - \frac{1}{4}\frac{\Delta x}{U\Delta t}\right) \leq C_{\text{odd}}(\pi) \leq U\left(1 + \frac{1}{6}\frac{\Delta x}{U\Delta t}\right)$$

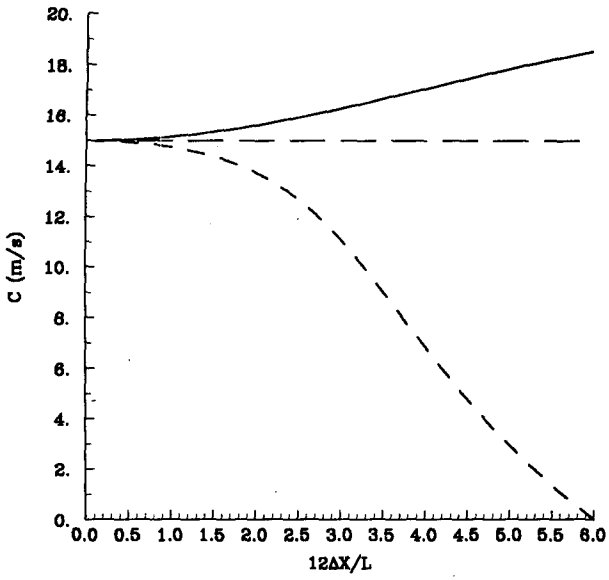

FIG. 11. Phase speeds for the one-dimensional advection problem. Curves are plotted for the noninterpolating semi-Lagrangian scheme (solid), the conventional centered time and centered space scheme (short dashed), and the analytic solution (long dashed) as discussed in the text.

when U' is positive, and

$$U\left(1 - \frac{1}{6}\frac{\Delta x}{U\Delta t}\right) \leq C_{\text{odd}}(\pi) \leq U\left(1 + \frac{1}{4}\frac{\Delta x}{U\Delta t}\right)$$

when U' is negative. Thus for all nonzero p, the numerical phase speed of the two grid-length wave is within a fraction $1/(4CN)$ of the analytic value U. Consequently the dispersion error for this NISL scheme is less than for the conventional CTCS treatment, and this bound on the dispersion error decreases as the (total) Courant number $U\Delta t/\Delta x$ increases. This behavior is attributable to the first term in (A6) and (A7), that is, the semi-Lagrangian advection to the grid point nearest the upstream point.

These properties are illustrated in Fig. 11, for which $U = 15$ m s^{-1}, $\Delta x = 200$ km and $\Delta t = 3$ h, giving $p = 2$, $U' = -3.52$, $U\Delta t/\Delta x = 0.81$ and $U'\Delta t/\Delta x = -0.19$. The phase speed is plotted as a function of $k\Delta x = 2\pi\Delta x/L$ where L is the wavelength. For convenience the abscissa is chosen to be $12\Delta x/L$, with 0 corresponding to $k = 0$ and 6 corresponding to the two grid-length wave. The solid curve represents (A6), the numerical phase speed for the NISL scheme, while the long dashed line shows the analytic phase speed U, and the short dashed line gives the numerical phase speed for the conventional CTCS scheme. Note that all three values agree for the longest waves, that the phase speeds for the NISL scheme exceed U for the shorter waves since U' is negative, and the values for the two grid-length wave are given by $p\Delta x/(2\Delta t) = 18.5$ m s^{-1} for the NISL scheme and zero for the CTCS scheme. This demonstrates that phase errors for the NISL scheme are smaller than those for the CTCS scheme due to the semi-Lagrangian advection to the nearest upstream grid point.

REFERENCES

Asselin, R., 1972: Frequency filter for time integrations. *Mon. Wea. Rev.*, **100,** 487–490.

Bates, J. R., and A. McDonald, 1982: Multiply-upstream, semi-Lagrangian advective schemes: analysis and application to a multi-level primitive equation model. *Mon. Wea. Rev.*, **110,** 1831–1842.

Krishnamurti, T. N., 1962: Numerical integration of primitive equations by a quasi-Lagrangian advection scheme. *J. Appl. Meteor.*, **1,** 508–521.

——, 1969: An experiment in numerical prediction in equatorial latitudes. *Quart. J. Roy. Meteor. Soc.*, **95,** 594–620.

Mahrer, Y., and R. A. Pielke, 1978: A test of an upstream spline interpolation technique for the advective terms in a numerical mesoscale model. *Mon. Wea. Rev.*, **106,** 818–830.

Mathur, M. B., 1970: A note on an improved quasi-Lagrangian advective scheme for primitive equations. *Mon. Wea. Rev.*, **98,** 214–219.

——, 1983: A quasi-Lagrangian regional model designed for operational weather prediction. *Mon. Wea. Rev.*, **111,** 2087–2098.

Ritchie, H., 1985: Application of a semi-Lagrangian integration scheme to the moisture equation in a regional forecast model. *Mon. Wea. Rev.*, **113,** 424–435.

Robert, A., 1981: A stable numerical integration scheme for the primitive meteorological equations. *Atmos. Ocean,* **19,** 35–46.

——, 1982: A semi-Lagrangian and semi-implicit numerical integration scheme for the primitive meteorological equations. *J. Meteor. Soc. of Japan,* **60,** 319–325.

——, T. L. Yee and H. Ritchie, 1985: A semi-Lagrangian and semi-implicit numerical integration scheme for multilevel atmospheric models. *Mon. Wea. Rev.*, **113,** 388–394.

Sawyer, J. S., 1963: A semi-Lagrangian method of solving the vorticity advection equation. *Tellus,* **15,** 336–342.

Verner, G., and R. Benoit, 1984: Normal mode initialization of the RPN finite element model. *Mon. Wea. Rev.*, **112,** 1535–1543.

Wiin-Nielsen, A., 1959: On the application of trajectory methods in numerical forecasting. *Tellus,* **11,** 180–196.